Total hadronic photoabsorption cross section on nuclei in the nucleon resonance region

N. Bianchi, V. Muccifora, E. De Sanctis, A. Fantoni, P. Levi Sandri, E. Polli, A. R. Reolon, and P. Rossi
Istituto Nazionale di Fisica Nucleare-Laboratori, Nazionali di Frascati, C.P. 13, I-00044, Frascati, Italy

M. Anghinolfi, P. Corvisiero, M. Ripani, M. Sanzone, M. Taiuti, and A. Zucchiatti
Istituto Nazionale di Fisica Nucleare and Dipartimento di Fisica dell'Universitá, Via Dodecaneso 33, I-16146 Genova, Italy
(Received 6 September 1995)

The total photoabsorption cross section for ^{7}Li, C, Al, Cu, Sn, Pb has been measured in the energy range 300–1200 MeV at Frascati with the jet-target tagged photon beam. A 4π NaI crystal detector and a lead-glass shower counter were used, respectively, to measure hadronic events and to reject the electromagnetic background. Data above 600 MeV clearly indicate a broadening of higher nucleon resonance peaks in nuclei and a reduction of the absolute value of the cross section per nucleon with respect to the free-nucleon case. This large broadening suggests a strong influence of the nuclear medium in the resonance propagation and interaction, while the systematic reduction of the measured cross sections might be due to a depletion of the resonance excitation strength and to the onset of the shadowing effect around 1 GeV. Moreover, our systematic study indicates that also the Δ-resonance excitation parameters are not the same for all nuclei, being its mass and width increasing with the nuclear density. [S0556-2813(96)00710-8]

PACS number(s): 25.20.Dc, 13.60.Hb, 14.20.Gk, 24.30.Gd

I. INTRODUCTION

The total photonuclear absorption cross section has been measured over broad mass number and photon energy ranges, yielding information on the influence of the nuclear medium on the intrinsic properties of nucleons in nuclei, as well as on the hadronic nature of the photon [1].

Between 140 and 500 MeV, the total cross section per nucleon clearly exhibits the presence of the $P_{33}(1232)$ resonance (Δ resonance) in nuclei. This is not a trivial statement considering the composite structures of the nucleon and the Δ resonance in terms of quarks and gluons: in general when such extended systems may overlap, their excitation spectra change as compared to the ones for isolated objects.

Previous data for various nuclei show that the shape and the strength of the resonances are nearly constant within the systematic errors of different experiments (which were typically of about 8–10 %), thus indicating an incoherent volume-photoabsorption mechanism. The average response of bound nucleons differs from that for the free nucleon, mainly because of the Fermi motion, the Pauli blocking, and the propagation and interaction of the Δ resonance in the nucleus. The process has been generally treated in the framework of Δ-hole models [2] where the total strength of the interaction is conserved. Moreover, it is worth mentioning that none of the experiments performed a systematic study of the process because each of them was only able to provide reliable data over a limited range of mass number. Then, differently from the pion-absorption experiments [3], in the study of the photon absorption no accurate experimental information was available on the possible influence of nuclear medium parameters like the size of the nucleus or the nuclear density on the first nucleon resonance excitation.

Until few years ago, much less information was available on the photoexcitation in nuclei of the higher mass nucleon resonances (N^* resonances): sparse data were collected at Yerevan with large acceptance over the actual photon energy and with fluctuations well above the experimental errors [4,5]. Recently, the total nuclear photoabsorption cross-section measurements carried out at Frascati with 200–1200 MeV tagged photons on ^{238}U [6], Be and C [7,8] have shown that in these nuclei the excitation peaks of the $D_{13}(1520)$ and $F_{15}(1680)$ resonances disappear, differently from the case in hydrogen [9] and deuteron [10], and that above 600 MeV there is a reduction of the absolute values of the cross section per nucleon with respect to those obtained from the deuteron data. On the contrary, the Δ-resonance peak is only slightly distorted in the nuclei, in agreement with the data available in the literature [1]. These experimental findings have been confirmed by the contemporary data on the photofission cross section of ^{238}U [11] and ^{235}U [12] obtained at Mainz up to 800 MeV.

This paper reports upon the complete analysis of the photoabsorption data obtained at Frascati on ^{7}Li, C, Al, Cu, Sn, Pb, using a tagged photon beam and the photohadronic method. In previous papers we published the preliminary and low statistic data obtained on C and CD_2 [8] and the average nuclear behavior [13] of the total photoabsorption cross section.

II. THEORY

A. Δ-resonance region

The dominant feature of photon interaction above the π threshold ($140<k<500$ MeV, being k the energy of the photon) is the Δ-resonance excitation. Consequently photon-induced nuclear reactions in this energy region depend directly upon the dynamics of Δ-resonance propagation through the nucleus. Pion-absorption and -scattering experiments suggested that this mechanism can be treated in the framework of a Δ-hole model in which the Δ resonance is generated as a quasiparticle, propagates in the nucleus and interacts with nucleons through an empirical complex nuclear potential composed by central and spin-orbit terms.

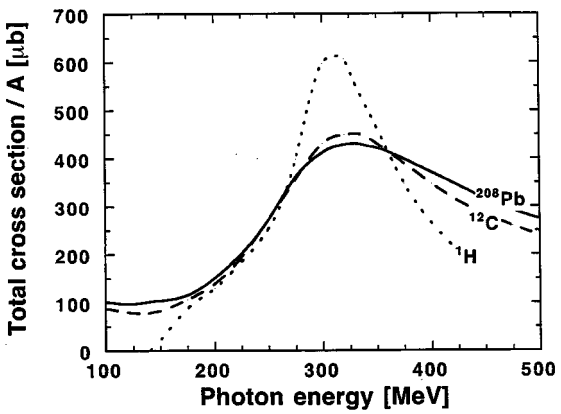

FIG. 1. Microscopical calculation for σ_A/A in the framework of a Δ-hole model: the dashed, solid, and dotted lines are the result for ^{12}C, ^{208}Pb, and the impulse approximation, respectively [14].

The former term is proportional to the nuclear density and its real part is responsible for the mass shift of the Δ resonance, while its imaginary part is responsible for the broadening of the Δ-resonance peak. The parameters of this complex potential are generally derived from the pion-nucleus elastic-scattering amplitude and have also been successfully used in the photon absorption and Compton scattering processes [2]. Differently from the pion, the photon penetrates freely into the nuclear volume, so that the cross section is expected to be roughly proportional to the mass number A.

Recently Carrasco and Oset [14] developed a microscopical model with a systematic many-body expansion in the number of Δ-hole excitations and with the inclusion of Pauli blocking, Fermi motion, and nonresonant absorption channels: in Fig. 1 we compare the results of their calculation for the free nucleon, carbon, and lead. As it is seen the reduction and the shift of the peak and the increasing of the width are larger for the heavier nuclei.

B. N^*-resonance region

The recent Frascati and Mainz photoabsorption data on nuclei above the Δ-resonance region ($k>500$ MeV) have triggered different theoretical attempts to describe the higher nucleon N^*-resonance behavior and justify why the elementary photonucleon absorption process is so widely modified inside the nuclei. Due to the large number of absorption channels and to the different dynamics and decay channels of N^* resonances, only simplified and very schematic models have been developed.

Kondratyuk *et al.* [15] tried to reproduce the experimental photofission cross section on ^{238}U [6] by using a simple phenomenological model where the produced resonance propagates inside the nucleus until it interacts with the surrounding nucleons. Due to these collisions, the mass and the width of the resonance increase in the nuclear matter. In order to reproduce the experimental data the authors found it necessary to use a higher collision cross section for the N^* resonances in the nuclei, producing a larger broadening of the D_{13} and F_{15} resonances with respect to the Δ resonance. Alberico *et al.* [16] found similar results by employing a simple resonance-hole model and assuming that the nuclear medium strongly increases the width of all resonances above the Δ resonance. In both approaches the strength of the excitation of Δ and N^* resonances is conserved but spread out over a wide energy range. These two models were able to reproduce our previous photofission cross-section data on ^{238}U, which can be assumed to be almost equal to the total cross-section ones.

Other approaches assumed that the excitation of nonspherical resonances (like the D_{13} and F_{15} resonances) are affected by the presence of surrounding nucleons, contrary to the case of the Δ resonance which is a simple internal spin-flip excitation of the nucleon. Using a nonrelativistic quark model with an oscillator potential that accounts for the quark exchange between the overlapping nucleons, Giannini *et al.* [17] have predicted a non-negligible depletion of the excitation strength of the higher mass resonances inside the nuclei (specifically an 11% of depletion for D_{13} resonance and 23% for the F_{15} resonance), when infranucleon distance is about 1 fm. On the contrary, Akulinichev *et al.* [18], employing a similar nonrelativistic quark model and short-range repulsion to analyze the suppression mechanism for the D_{13}-resonance excitation due to the overlap of nucleons, concluded that this effect should be negligible.

C. Shadowing region

At energies above the nucleon resonance region ($k>2$ GeV) the absorption of photons in nuclear matter has been generally considered on the vector-meson dominance (VMD) assumption, in which the photon first converts itself into a vector meson V and then interacts with hadronic matter. The shadowing effect arises when a photon of energy k fluctuates into a vector meson of mass m_V and propagates for a length $l_V=2k/m_V^2$ close to the nuclear dimension so that there is a non-negligible probability that its interaction is hadroniclike. Earliest simple VMD models [19,20] considered the photon as a superposition of a bare photon and the low-lying vector mesons $V=\rho,\omega,\phi$ and were able to reproduce the photonuclear absorption cross-section behavior in the few GeV domain: they predicted a 10–20 % shadowing effect around 2–3 GeV. More sophisticated models (generalized vector dominance) [21,22] included higher mass vector mesons and nondiagonal terms in order to better explain higher-energy photoabsorption data and virtual photon absorption in deep-inelastic electron scattering. Recently Piller *et al.* [23] assumed, for the intermediate hadronic state, the mass spectral function related to the cross section of the $e^+e^-\rightarrow$*hadrons* processes, which includes at low energy the $\pi^+\pi^-$ nonresonant production and the low-energy tail of the broad ρ meson peak. These low-mass hadronic components could lower the energy threshold for shadowing which then results significant at energy as low as 1 GeV, i.e., in the nucleon resonance region.

Finally, it is worth mentioning that about 20 years ago, Weise provided a sum rule which, employing a dispersion relation approach to reconcile the data for the enhancement factor value observed in the photoabsorption below 140 MeV and the shadowing effect observed above 2 GeV, suggested a strong nuclear medium effect in the whole resonance region [24].

In order to disentangle from these and other possible explanations, one needs an accurate knowledge of the absolute

value of the photoabsorption cross section in the nucleon resonance region, over a broad range of mass numbers.

III. EXPERIMENT

The measurements were carried out at Frascati using the jet-target tagged photon beam [25]. Details of the facility are described elsewhere [8,26].

The total photoabsorption cross section on nuclei was measured using the photohadronic technique. This technique provided a direct and absolute determination of the photoabsorption cross section by measuring the production rate of hadronic events, and rejecting the preponderant electromagnetic events mainly by an angular separation. In fact, while the hadronic events are more largely distributed in angle, the electromagnetic event distribution is strongly peaked in the forward direction and therefore can be suppressed by using a high efficiency electromagnetic shower detector as a veto counter.

A. Detectors

As a hadron detector (HD) we used a cylindrical NaI crystal annulus (32 cm long, 15 cm thick, and 5 cm of internal diameter) made of three sectors surrounding the target.

With the target set in the center of the detector, the angular coverage was $9°<\theta<171°$ for the polar angle and almost 2π for the azimuthal one (which correspond to more than 98% of total coverage in the laboratory system). Light-emitting diodes installed on each crystal allowed to monitor regularly the gain stability. The HD provided a good measurement of the final-state total energies for the hadronic events, which were remarkably higher than those for the electromagnetic events in the solid angle defined by the HD detector.

The shower detector (SD) set about 70 cm downstream the target, consisted of a dense SF6 lead-glass cylinder, 30 cm long and 12 cm in diameter. The large detector thickness (19 radiation lengths) provided an efficiency equal to one for detecting electromagnetic showers; moreover, its good energy resolution (σ/E) (better than 5% for 1.2-GeV photons) made it possible to set the threshold appropriately and safely. The stability of the SD response was periodically checked by monitoring in coincidence the peak positions of four tagging channels. A lead collimator, 20 cm long and 8 cm diameter, was placed between the HD and the SD for defining a maximum polar angle of 4.2° for electromagnetic events at the target center. Moreover the Cerenkov light emission process in the SD provided a good rejection of the low-energy hadrons which might reach the SD.

B. Targets

We used solid targets in the form of circular disks, 3 cm in diameter and thickness about $0.1X_0$ for C, Al, Cu, Sn, and Pb and $0.025X_0$ for Li, X_0 being the radiation length (the actual thicknesses are given in Table I). The targets were individually mounted on frames and moved into and off of the photon beam. Due to the finite thickness, T, of the target the effective photon beam was partially attenuated by electromagnetic interaction: specifically the average photon transmission before the hadronic interaction was

TABLE I. Targets, thicknesses, number of collected events (#) ($\times 10^3$), and overall average corrections δ for each target and electron beam energy E_0 (GeV).

Target	Thickness (g/cm^2)	$E_0=0.73$		$E_0=0.85$		$E_0=1.2$		$E_0=1.5$	
		#	δ	#	δ	#	δ	#	δ
Li	1.996±0.029			13	10%			18	6%
C	3.452±0.014	25	11%	20	10%	18	7%	19	7%
Al	2.408±0.009	15	12%	12	11%	13	7%	13	7%
Cu	1.272±0.009	10	13%	9	11%	13	8%	11	7%
Sn	0.892±0.007	9	13%	12	11%	11	8%	10	7%
Pb	0.658±0.023	8	10%	10	11%	7	8%	17	8%

$$\frac{n(T,\mu)}{n(0,\mu)}=\frac{1-e^{-\mu T}}{\mu T}, \tag{1}$$

where μ is the photon attenuation coefficient. The calculated values of the average photon transmission for this experiment ranged from 99.1% for Li to 96.5% for heavier nuclear targets. Additional runs with different thicknesses ($0.025X_0$ and $0.05X_0$) did not show any additional thickness effect.

In order to reduce possible effects due to changes of stored electron beam, data for all the targets were collected for each fill of the machine and the electrons were always reinjected into the storage ring only after the completion of one or more measurement cycles. Empty-target measurements were regularly interspersed inside a complete cycle of solid-target runs and then subtracted. The empty-target yield was roughly equivalent to ~ 0.8 g cm^{-2} of carbon, which amount to about 20% of the total event yield. This background could be mainly ascribed to the interactions on the windows, on the air along the beam path before the target, and on the target frame. The number of collected events and the off-line corrections for the different energies are given in Table I.

C. Electronics

The signals from the 16 tagging channels in coincidence with the SD, were recorded on scalers providing the photon beam flux $N_\gamma(k)$. The hadronic events $N_H(k)$ were signed by the coincidence between the tagging and the HD signals, vetoed by the SD signal above a threshold fixed for each energy. They were also counted with an additional scaler. The random coincidences on both coincidences due to the electron beam time structure were on-line measured and subtracted. After this subtraction we obtained the yield $Y(k)$, derived from the scaler counts as follows:

$$Y(k)=\frac{AN_H(k)}{N_A\rho x N_\gamma(k)}, \tag{2}$$

where A is the mass number, N_A is the Avogadro number, ρx is the target thickness.

D. Measurement

We covered the photon energy range from 300 to 1200 MeV with four different electron beam energies $E_0=1500$ MeV, $E_0=1200$ MeV, $E_0=850$ MeV, $E_0=730$ MeV, which

ensured large overlapping regions of photon energy. Running conditions, such as HD and SD discriminator thresholds, were adjusted to optimize the efficiency of hadron detection and of the electromagnetic suppression for the different beam energies. The random to true coincidence ratio was maintained ~10% by keeping the tagged photon beam at a constant rate of $\sim 10^4$ photons/s. Moreover we checked the random coincidence subtraction procedure by deriving the yield at very different photon intensities: no additional rate effect was found when changing the intensity of tagged and untagged photons up to a factor of 5.

IV. PROCEDURE AND RESULTS

The yields were very close to the absolute values of the total cross section. In fact, small off-line corrections were needed to account for (i) the loss of hadronic events emitted in the forward hole of the HD or with energy below the HD threshold, (ii) the HD contamination due to electromagnetic events which give signals above the HD threshold and are not vetoed by the SD, and (iii) the loss of hadronic events due to pulse heights above the SD threshold simulating e.m. events.

In order to properly calculate these corrections, particular care was devoted to study the apparatus response function.

Photoproduction of hadronic events on the target, was simulated by using a Monte Carlo program based on a cascade-evaporative model [27]. This code describes the photon interaction with nucleons through the quasideuteron process and the one-pion and two-pion production processes in resonant and nonresonant states and thus can be applied to the photoabsorption of up to 1.2 GeV photons. Hadrons photoproduced and residual nucleus excitation are the output of the cascade stage of the photonuclear interaction; successively the excited residual nucleus emits low-energy evaporation nucleons or light nuclei.

The response function of the hadron detector to the generated hadronic events was studied with a GEANT-3 code modified to correctly take into account the hadronic cross section in NaI for protons, neutrons, and charged pions. This code was implemented with the inclusion of the energy-range tables in NaI for protons and pions at energies below 1 GeV [28]. Figure 2 shows the simulated HD response functions to the hadrons photoproduced on C by 600–1200 MeV photons. The spectrum shows a broad peak at ~200 MeV, which is due to hadronic events with at least one pion in the final state, while the structure around 80 MeV is due to the small fraction of events with no pion in the final state. Also shown in the figure is the measured spectrum which results in good agreement with the hadronic simulation above the threshold. Under the threshold the measured spectrum is higher because it also included electromagnetic events.

We also simulated the electromagnetic processes with a modified version of the GEANT-3.13 code which correctly accounts for the measured angular distribution of pair production in the energy range of interest both in nuclear and atomic fields. Moreover, we also implemented the GEANT-3.13 code with the Cerenkov photon emission, the attenuation in the lead glass of the Cerenkov light, and the spectral response of the photomultiplier tube (PMT).

Monte Carlo corrections for the finite angular acceptance

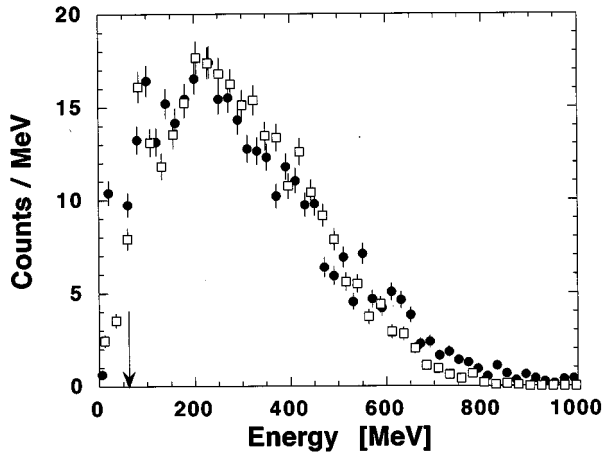

FIG. 2. Comparison between the simulated (open squares) and measured (solid circles) response functions of the hadron detector to 600–1200 MeV photons on carbon target. The arrow indicates the threshold setting.

of the HD and for the possible contamination due to the electromagnetic events not vetoed by the SD, were experimentally tested by varying the HD solid angle; this was performed by moving upstream and downstream the targets inside the HD. Figure 3 shows the average yields measured at two beam energies ($E_0 = 1.5$ GeV and $E_0 = 0.85$ GeV) for different tin-target positions, as a function of the uncovered forward solid angle $\simeq 2\pi\theta^2$, which corresponds to the forward hole of the HD. The arrow indicates the missing solid angle for the target at the center of the HD, that corresponds to the standard position used for the cross-section measurements. The Monte Carlo predictions have been parametrized by a function of the form $a - b\theta^2 + (c/\theta^2)$, where a is the total hadronic cross section for an ideal 4π hadron detector, $-b\theta^2$ represents the loss of hadronic events in the forward hole of the HD, and $+c/\theta^2$ represents the contamination of electromagnetic events due to the e^+e^- pairs produced in the target. As shown, the latter becomes relevant only when the target is moved very upstream to positions which correspond to very small θ^2 values and the HD solid-angle coverage approaches 4π. The values deduced from this measurement for both these corrections well agree with the predictions of the Monte Carlo calculations.

The rejection efficiency due to the angular acceptance of the SD was also evaluated by changing the radius of the collimator placed in front of it and compared with the Monte Carlo prediction. Figure 4 shows the average yields from a tin-target measured at two electron beam energies ($E_0 = 1.5$ GeV and $E_0 = 0.85$ GeV) as a function of the forward solid angle $\simeq 2\pi\theta_s^2$ covered by the SD. The arrow indicates the standard solid angle for the cross-section measurements. The two curves, that represent the Monte Carlo predictions, have been parametrized as $d + e/\theta_s^2$ and well agree with the experimental points. As it is shown, the hadronic cross section d is constant in a wide range of forward angles thus indicating that the electromagnetic events were adequately and safely suppressed by the veto counter. The increase of the yields predicted for small angles (e/θ_s^2 term) is ascribed to the low-energy showers generated inside the collimator, which produce a signal below the SD veto threshold.

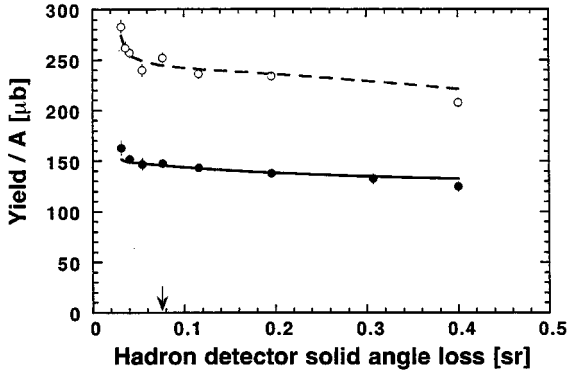

FIG. 3. The average yields measured on the tin target for two electron beam energies with different solid-angle coverage of the HD. Open and solid circles refer to $E_0=850$ MeV and $E_0=1500$ MeV measurements, respectively. The dashed and the solid lines are the relevant MC predictions. The arrow indicates the solid angle loss relevant to the measurement position.

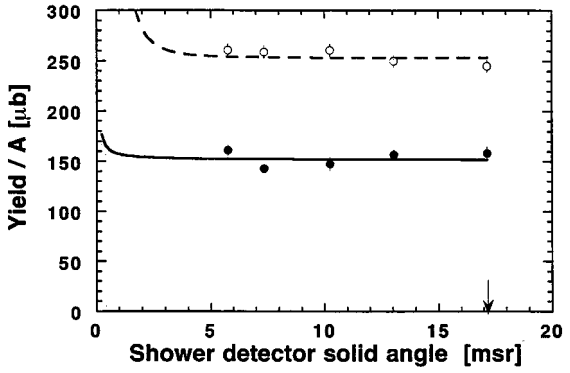

FIG. 4. Same of Fig. 3 but with different solid angle coverage of the SD. The arrow indicates the solid angle relevant to the measurement position.

The good agreement between the Monte Carlo predictions and the experimental results confirms a high reliability of the calculated corrections for both the hadronic and electromagnetic events. Table I lists the average values of the Monte Carlo corrections with respect to the yields, for the different energies and for all the studied nuclei.

In Fig. 5 the comparison between the yield and cross section is shown for the aluminum target, together with the total software corrections: the latter decrease from about 15 to about 5 % while the energy increases.

In Table II are given the total cross-section values normalized to the mass number A for the six studied nuclei together with the statistical errors. Also given are the weighted averages of data points which can be considered as the cross sections on an ''average nucleus'' with $Z/A=0.465$, $N/A=0.535$, density $\rho=0.101$ nucleons/fm^3 and Fermi momentum $p_F=232$ MeV/c, i.e., an ''aluminumlike'' nucleus. The plots of these data are shown in Fig. 6 with statistical errors only, while systematics errors are represented by the bands in the bottom.

Good overlaps were observed between the data collected at different energy sets, and this evidenced the good control of the systematic errors. These were essentially due to uncertainties in the photon beam flux ($\simeq$2%), the target thickness ($\sim$0.5–1.5 %) and mainly the calibration and threshold efficiency of both the shower and hadron detectors (above 600 MeV this contribution is constant with energy and increases from $\simeq$2% to $\simeq$6.5% with the target mass number A, while, in the Δ-resonance region, where it depends both on energy and A, it varies from $\simeq$4.5% to $\simeq$7.5%). In conclusion, the total systematic errors increase with A from $\simeq$3% to $\simeq$7% in the D_{13}- and F_{15}-resonance regions and vary from $\simeq$5% to $\simeq$8% in the Δ-resonance region.

V. ANALYSIS AND DISCUSSION

Total photonuclear cross sections can be considered as a convolution of resonant and nonresonant production processes on individual nucleons smeared by nuclear medium effects. To extract informations on the latter ones, we adopted the phenomenological procedure previously used by some of us [15]: we first determined the resonance masses, widths and excitation strengths by fitting the proton and neutron data, then we fitted the nuclear data using the same analytical expression with some free parameters. With respect to the previous procedure we adopted the following improvements: we used a better Breit-Wigner parametrization of the resonances, a more accurate determination of neutron cross-section values from the deuteron data, a different nonresonant pionic background parametrization, and more precise nuclear densities. Moreover we also considered the contribution of quasideuteron background, of nuclear effects (like resonance mass shifts and suppression), and of the shadowing effect.

A. Free-nucleon parametrization

In order to determine the resonance masses W_r, widths Γ_r, and strengths I_r, we fitted the proton data available in the literature [9,29] to a sum of six Breit-Wigner resonances plus a smooth background. The six resonances parametrized in the fit can be identified as the $P_{33}(1232)$ (Δ resonance), $P_{11}(1440)$, $D_{13}(1520)$, $S_{11}(1535)$, $F_{15}(1680)$, and $F_{37}(1950)$, which give the main contribution to the total γN cross section. We expressed the Breit-Wigner resonances in the form given by Walker [30] which is correct at least for the one-pion-decay channel:

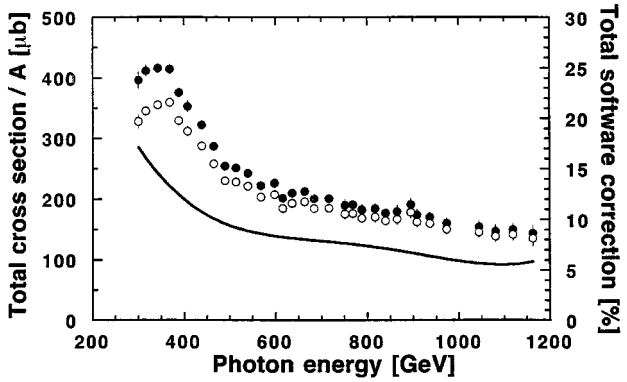

FIG. 5. Aluminum yields (open circles) and cross sections (solid circles), on the left scale. The amount of the total correction due to hadronic losses and electromagnetic contamination (solid line), on the right scale.

TABLE II. Total cross-section values normalized to the mass number A for the studied nuclei. Also indicated are the statistical errors. The average is computed weighting each nucleus cross-section datum with its statistical error.

k (GeV)	^{7}Li (μb/A)	C (μb/A)	Al (μb/A)	Cu (μb/A)	Sn (μb/A)	Pb (μb/A)	Average (μb/A)
0.301		420±10	397±13	375±16	398±19	387±21	401.5±6.5
0.317		430±7	412±9	430±12	419±14	381±15	419.5±4.6
0.343	440±15	432±6	416±8	403±10	417±11	415±12	421.2±3.6
0.369	389±10	406±6	414±8	413±13	413±10	410±12	407.1±3.6
0.389	351±12	393±6	376±8	376±8	399±11	389±10	383.6±3.4
0.408	324±13	362±7	353±9	358±12	378±13	329±14	354.7±4.1
0.439	282±9	324±6	323±7	317±9	328±10	337±15	317.8±3.3
0.465	257±13	287±5	288±7	294±9	322±10	319±12	292.0±3.2
0.490	244±12	251±5	255±7	252±8	250±9	257±11	251.6±3.2
0.514	223±12	254±4	251±5	247±6	241±8	273±9	250.9±2.5
0.540	194±7	235±3	243±4	236±5	245±6	249±7	235.7±2.0
0.568		216±6	222±7	219±9	228±11	240±13	221.1±3.6
0.598	222±11	218±6	227±7	212±9	222±10	210±12	218.8±3.4
0.616	211±6	200±5	202±6	197±8	210±9	197±8	202.6±2.7
0.636	196±6	210±4	211±5	201±6	203±7	192±8	204.2±2.3
0.664	213±7	207±4	213±5	198±7	207±7	191±7	206.4±2.2
0.684	205±7	190±6	201±8	192±7	181±10	174±9	192.4±3.0
0.717	206±8	185±5	201±6	186±7	171±9	173±9	188.4±2.7
0.751	194±9	181±7	190±9	175±10	207±9	159±12	186.0±3.6
0.768		195±5	191±6	179±8	178±13	187±12	189.8±3.2
0.788	166±7	184±7	183±9	174±12	173±13	173±12	176.3±3.6
0.817	180±9	183±7	185±9	163±12	187±14	178±12	180.3±3.9
0.840	194±8	187±5	178±6	179±8	180±10	182±11	183.7±3.0
0.865		181±8	180±10	172±12	179±16	218±21	181.1±4.9
0.895		182±7	192±10	164±12	169±15	195±14	181.3±4.7
0.908	169±8	162±7	174±9	169±13	182±12	167±15	169.1±3.9
0.936	137±7	166±5	171±7	160±10	162±13	168±12	160.3±3.2
0.973	171±8	178±7	161±9	157±12	151±13	171±12	168.2±3.8
1.044	145±9	167±7	155±9	164±13	158±15	151±14	157.2±4.1
1.081	165±10	147±7	147±10	148±15	148±17	147±15	150.9±4.4
1.119	147±8	156±7	150±10	143±14	154±16	163±15	151.6±4.1
1.163	140±12	144±10	144±13	145±20	120±22	135±20	140.7±5.7

$$I = I_r \left(\frac{K}{K_r} \right)^2 \frac{W_r^2 \Gamma \Gamma_\gamma}{(W^2 - W_r^2)^2 + W_r^2 \Gamma^2}, \tag{3}$$

where

$$\Gamma = \Gamma_r \left(\frac{q}{q_r} \right)^{2l+1} \left(\frac{q_r^2 + X^2}{q^2 + X^2} \right)^l, \tag{4}$$

$$\Gamma_\gamma = \Gamma_r \left(\frac{K}{K_r} \right)^{2J\gamma} \left(\frac{K_r^2 + X^2}{K^2 + X^2} \right)^{J\gamma}, \tag{5}$$

and W is the c.m. energy; K and q are the momenta of the photon and single-pion decay in the c.m. frame, and the suffix r refers to the values at the resonance mass W_r; J_γ and l are their angular momenta. The damping parameter X for free protons was set equal to 0.35 GeV for all the resonances except for the Δ resonance for which the value $X = 0.15$ was used.

To take into account the nonresonant one-, two- and multipion production, we also considered in the fit a background parametrization of the simple form:

$$\sigma_B = (a_1 + a_2 k^{-1/2})(1 - e^{-2(k-k_0)}) \tag{6}$$

which has the correct Regge energy asymptotic behavior and include the pion photoproduction threshold energy k_0. The values a_1 and a_2 were fixed by matching with the results of high-energy data ($k \geq 2$ GeV) [9] resulting for the proton $a_1^p = 91$ μb, $a_2^p = 71$ μb GeV$^{1/2}$. Therefore the fit function was

$$F = \sum_r I(I_r, W_r, \Gamma_r) + \sigma_B(a_1, a_2). \tag{7}$$

In Fig. 7(a) it is shown the comparison between data on proton and the fit, together with the single contributions of the different resonances and background.

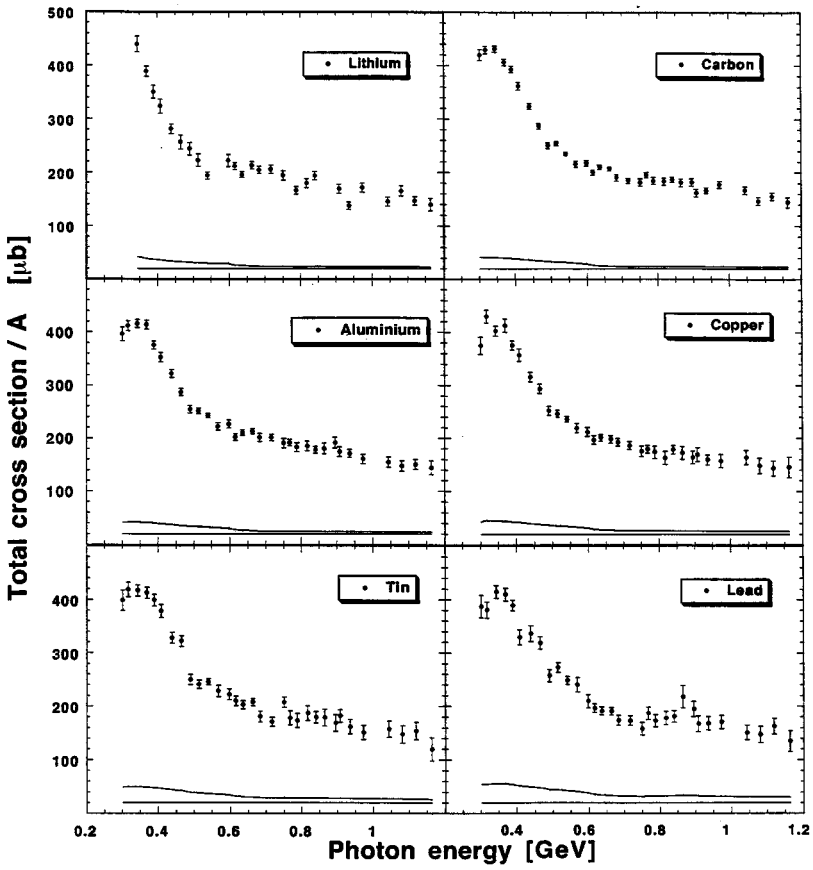

FIG. 6. Total cross section for the six nuclei. The error bar represents the statistical error. The band at the bottom of each plot represents the systematic error.

In order to extract the total cross section on free neutron we performed a fit to the deuteron data [10,29]. In this fit we used the same parametrization as for the proton plus an additional nonresonant photodisintegration cross section background which gives a non-negligible contribution mainly in the Δ-resonance region; this has been extracted from total photodisintegration cross-section data and resulted well in agreement with the theoretical prediction which include meson exchange current with no isobar terms [34]. More details about this nonresonant photodisintegration contribution will appear in a forthcoming paper. The nonresonant pionic background parameter resulted for the deuteron $a_1^D = 175$ μb, $a_2^D = 135$ μb GeV$^{1/2}$ and were derived from high-energy data [10]. Moreover we assumed $W_r^n = W_r^p$ and $\Gamma_r^n = \Gamma_r^p$, while the resonance couplings I_r, which in principle could be different, were derived from deuteron and proton resonance parameters as follows:

$$I_r^n = \frac{I_r^D \Gamma_r^D - I_r^p \Gamma_r^p}{\Gamma_r^n}. \tag{8}$$

Then the neutron cross section has been derived from the experimental deuteron and proton data:

$$\sigma^n = \sigma^d \frac{F^p + F^n}{F^D} - \sigma^p. \tag{9}$$

This is shown in Fig. 7(b) together with the fit performed on the neutron data.

The resonance parameters W_r, Γ_r, and I_r deduced from the proton and deuteron fits and I_r derived for the neutron are shown in Table III.

Figure 8 shows the integrated strength values, $\Gamma_r I_r$, for proton and neutron provided by our fit, together with the values calculated by Armstrong *et al.* for the proton [9] and the ranges given by the Particle Data Group (PDG) [32]. This comparison shows general good agreement between the values obtained from our fit and those given by the PDG and point out the improvement respect to the Armstrong *et al.* results for resonances higher than the Δ resonance. Moreover, we found that the Δ- and D_{13}-resonance excitation strengths are approximately the same for the proton and the neutron, while the F_{15}-resonance amplitude is strongly suppressed in the neutron in agreement with the quark model predictions for the electromagnetic coupling of the resonances. The remaining three resonances are less excited and less well defined. Their parameters are more dependent on the background parametrization but the values we found are still consistent with the PDG values.

B. Nuclear medium effects

The resonance parameters obtained from the fits to the free-nucleon data shown in Table III are a suitable input for the fit to the bound nucleon data. In order to extract information about the resonance behavior in nuclei, we considered the following processes.

(i) The quasideuteron process, which was parametrized using the Levinger expression [33]:

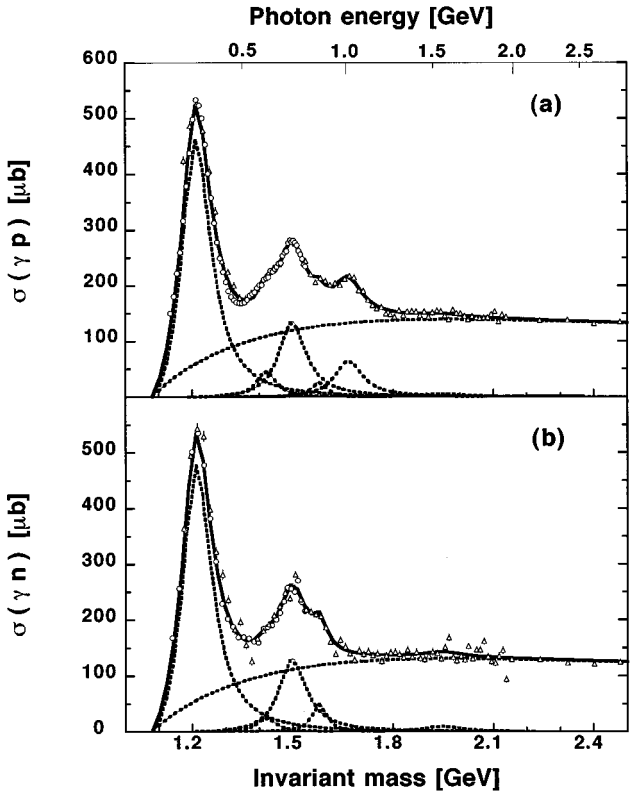

FIG. 7. (a) Total cross section measured on proton: open circles [29] and triangles [9]. The solid line is the result of our fit; the dotted lines are the resonant and nonresonant contributions. (b) The same for the neutron; neutron data are derived with the procedure described in the text.

$$\sigma_{\mathrm{QD}} = L \frac{NZ}{A} e^{-D/k} \sigma_D , \tag{10}$$

where k is the photon momentum, L is the Levinger factor, $D = 0.06$ GeV is a damping factor, and σ_D is the nonresonant photodisintegration cross section on the deuteron. Within this parametrization isobar degrees of freedom are included in the Breit-Wigner term only.

(ii) The Fermi motion, which produces a smearing of the resonance peak by increasing its width and suppressing its maximum of a quantity S_F depending on the Fermi energy of the nucleus ($\epsilon_F = 20-40$ MeV). This approximation has been shown to be valid in the description of nucleon resonances in nuclei where the peaks are hundreds of MeV broad, that is about 1 order of magnitude bigger than the kinetic energies of nucleons inside the nucleus [15]. This effect has found to increase the resonance full widths in nuclei of about 10–15 %.

(iii) The Pauli blocking, which arises because of the occupation by other nucleons of the momentum space below the Fermi momentum, thus reducing the space phase available for the resonance decay products. This effect increases the resonance lifetime and decreases its width of a quantity B_P identified with the solid angle formed in the resonance rest frame by the allowed nucleon directions [15]. For an average density nucleus, B_P is computed to be 0.77 for the Δ resonance and about 0.90 for higher resonances.

TABLE III. Resonance masses W_r, widths Γ_r, and strengths I_r for proton (p), neutron (n) and deuteron (d) derived from the hydrogen and deuterium data. Masses and widths for neutron have been assumed equal to the proton ones.

	W_r (MeV)		Γ_r (MeV)		I_r (μb)		
Resonance	p	d	p	d	p	n	d
$P_{33}(1232)$	1230	1241	122	161	415	429	639
$D_{13}(1505)$	1505	1502	100	134	133	128	195
$F_{15}(1680)$	1671	1680	100	110	65	0	59
$P_{11}(1440)$	1423	1413	66	81	47	25	59
$F_{37}(1950)$	1954	1974	150	165	5	8	12
$S_{11}(1535)$	1580	1570	50	73	27	49	52

It is to point out that the (ii) and (iii) contributions partially compensate for each resonance.

(iv) The propagation and interaction of the resonance in the nuclear medium which reduces the lifetime of the photoproduced resonance thus increasing its width. In analogy with the Δ-resonance propagation in nuclei, the medium effects on the N^*-resonance propagation have been described by a phenomenological potential whose real and imaginary parts are related to the shift of the mass δM and to the broadening $\delta\Gamma$ of the resonance. Introducing an optical pseudopotential for the N^*N interaction, δM and $\delta\Gamma$ are proportional to the real and imaginary part of the forward N^*N scattering amplitude $f_{N^*N}(0)$ and to the density of the nuclear medium ρ_0:

$$\delta M = -\frac{2\pi}{M} \mathrm{Re} f_{N^*N}(0) \rho_0 , \tag{11}$$

$$\delta\Gamma = \frac{4\pi}{M} \mathrm{Im} f_{N^*N}(0) \rho_0 . \tag{12}$$

Using the optical theorem we deduced

$$\delta\Gamma = \rho_0 \sigma^* v \gamma , \tag{13}$$

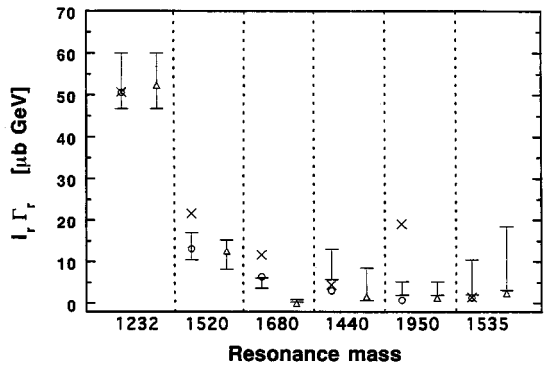

FIG. 8. Product of the strength at the mass by the width for the main six nucleon resonances. Circles and triangles are the values we derived by fitting the proton [29,9], and the neutron data [29,10], respectively; crosses are the values provided for the proton by Armstrong *et al.* [9] and vertical lines are the PDG ranges [32].

where v is the propagation velocity, γ is the Lorentz factor, and σ^* is the total cross section of the resonance-nucleon interaction.

More details of these nuclear effects and their influence on the resonances behavior in the nuclear medium, have been described elsewhere [15].

Taking into account the above-listed processes, each resonance in the nuclear medium was parametrized by a total width Γ and mass M:

$$\Gamma = \frac{\Gamma_r B_P + \delta\Gamma}{S_F}, \tag{14}$$

$$M = W_r + \delta M. \tag{15}$$

In the fits to the total cross sections on nuclei we used W_r, Γ_r, and I_r obtained from the fit to the proton and neutron data, and the computed values for B_P and S_F, while $\delta\Gamma$ (or $\sigma^* v$) and δM were free parameters. In order to decrease the total number of free parameters we assumed $\delta M = 0$ for all the resonance except for the Δ resonance. This because the Δ resonance in the nuclear medium is dominant and much narrower than the other resonances and even a small shift of its mass contributes very significantly to the χ^2 value. Moreover, we used only two $\delta\Gamma$ as free parameters: one for the Δ resonance and a common one for all other resonances. As our data cover the mass range $1.20 < W < 1.75$ GeV, in order to cover the whole Δ-resonance energy region, we used data available from previous experiments in the range $1.14 < W < 1.20$ GeV, so that the lower limit is the same as for the proton and neutron data fit. Specifically, we used lithium data [34] for lithium, carbon data [35,36] for light nuclei, and lead data [36] for heavy nuclei.

In the energy range explored it is expected that the photonuclear cross section changes smoothly with the macroscopic nuclear parameters like the density or the mass number. Moreover, as it will be discussed later, we found necessary to include in the model a reduction mechanism of the cross section in order to reproduce the data at higher energies. Therefore, we first derived the ΔN and $N^* N$ cross sections through an accurate comparison of the models to the data, and then studied the dependence on the nuclear density. In order to provide the better determination of these cross sections, which are independent from nuclear parameters, we used the ''average nucleus'' data as a typical nuclear photoabsorption data.

The results of the fit to the ''average nucleus'' total cross sections are shown in Fig. 9 together with the separate resonant, quasideuteron, and background contributions. The best description of the data was found for $\delta M_\Delta = 38 \pm 1$ MeV and $\sigma^* v_\Delta = 35 \pm 1$ mb, for the Δ resonance and $\sigma^* v_{N^*} = 135 \pm 5$ mb in average for the other N^* resonances. While the $\sigma^* v_\Delta$ value is in fair agreement with the one derived from the $NN \to \Delta N$ processes, the value found for the other resonances violate the unitarity limit which requires $\sigma^* v_{N^*} \leqslant 80$ mb [15].

To better investigate the broadening and the shift of resonance structures we studied the ratio of the bound nucleon to free-nucleon cross sections which strongly depends on these effects. In particular either a broadening or a shift produce an oscillating behavior of this ratio. Figure 10(a) shows the ratio

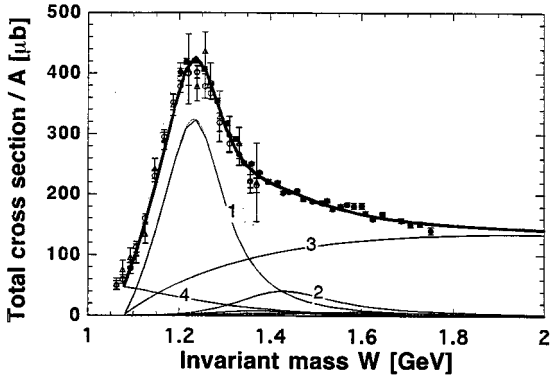

FIG. 9. Total cross-section data: our data on the average nucleus (solid circles) are compared with previous data on C (open circles) and Pb (open triangles) measured with a similar experimental technique [36]. Also shown are the phenomenological fit (thick line) and the resonant and nonresonant separate contributions (thin lines) of the P_{33} (1) and D_{13} (2) excitation, pionic background (3) and quasideuteron background (4).

between the measured ''average nucleus'' data and the fit to the free nucleon, together with the ratio computed with the above-described model. Also shown are the prediction of the model in the case of no shift for the Δ resonance ($\delta M_\Delta = 0$) and no broadening ($\delta\Gamma_\Delta = \delta\Gamma_{N^*} = 0$) due to the resonance interaction (Pauli blocking and Fermi motion only): as it is seen the propagation and interaction of resonances are really needed to explain the data up to 1.2 GeV. Moreover, from the figure it results that the used resonance broadening leads to an antishadowing behavior at higher energies with a large overestimate of data above 2 GeV [37].

The violation of the unitarity limit and the antishadowing behavior can only be cured introducing an effective reduction of the cross section in the resonance region. Two processes have been suggested to justify this reduction: (i) the existence of a dynamical mechanism which partially inhibits the excitation of nucleon resonances in nuclei, causing a reduction of I_r in nuclei [17]; (ii) the onset of nuclear shadowing [38], which causes a reduction of the total cross section. It is worth pointing out that in the framework of this model no resonance effects are considered.

Solid line of Fig. 10(b) shows how the inclusion of these two effects makes it possible to cure the discrepancy with data at high energy. Moreover, in this case, the cross section ΔN remains almost unchanged, being $\sigma^* v_\Delta = 34 \pm 1$ mb, while the one for higher resonance is strongly reduced, resulting $\sigma^* v_{N^*} = 80 \pm 4$ mb, in reasonable agreement with the unitarity limit.

Finally Fig. 11 shows how well the average values of our result on C and Pb in the F_{15}-resonance energy region agree with the low-energy prediction of a recent shadowing model [38], while older and simpler shadowing models give very different evaluations of the shadowing threshold region around 1 and 2 GeV, mainly due to different ρ meson cross-section parametrization [19,20]. Shadowing effect is quantitatively evaluated by the parameter $A_{\text{eff}}/A = \sigma_A/(Z\sigma_p + N\sigma_n)$ which represents the effective number of nucleons seen by the incoming probe.

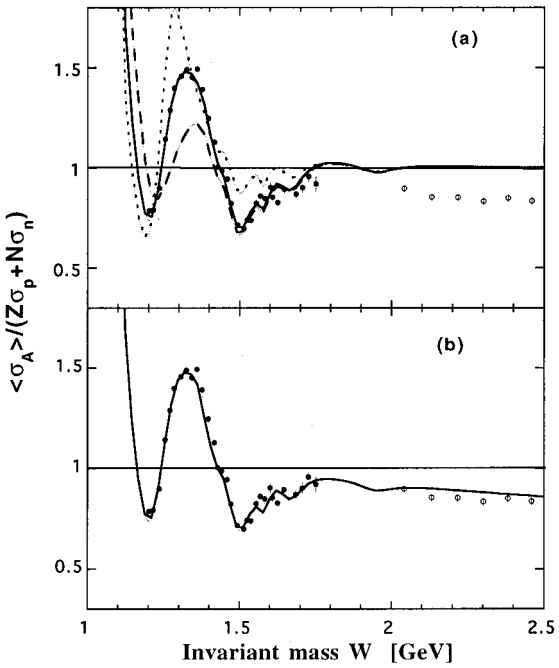

FIG. 10. (a) Ratio between cross section on the average nucleus and that on a free nucleon: our data are indicated by solid circles while Daresbury data [37] by open circles. The solid line is the result of the phenomenological model described in the text which considers Fermi motion, Pauli blocking, and resonance propagation and interaction; the dashed line is the result of the model with $\delta M_\Delta = 0$ (no Δ-resonance mass shift) while dotted line with $\delta\Gamma = 0$ (no resonance interaction). (b) The same as (a): the solid line is the phenomenological model with the inclusion of shadowing effect and a partial damping of resonances.

C. Nuclear density effect

As previously mentioned, nuclear medium effects are generally expected to depend on nuclear parameters like the average nuclear density $\rho(A)$ or the mass number A. To check this expectation we fitted the total cross-section values obtained on different nuclei for each invariant mass W with a linear function of the nuclear density $\sigma_A(W)/A = b(W)[1+\beta(W)\rho(A)]$. In the fits we assumed that the average nuclear densities were $\rho(A) = 3A/4\pi R^3$ with $R^2 = 5\langle r^2\rangle/3$, $\langle r^2\rangle$ being the rms electron-scattering radius of the nucleus [41].

In Fig. 12 are shown all the linear coefficient values, $\beta(W)$, obtained from our data together with the ones obtained from the data measured at higher energies on the same nuclei [9], except the lithium. As shown the qualitative energy behavior for the $\beta(W)$ parameter is very close to the one obtained for the ratio of cross sections shown in Fig. 10, thus experimentally indicating that nuclear medium effect really increases with the nuclear density, at least up to the D_{13}-resonance region. In the F_{15}-resonance region, where the nonresonant background is large and where many resonances overlap, no definite indication can be derived.

It is worth mentioning that we also fitted our data to a power law $\sigma_A(W)/A = a(W)A^{\alpha(W)}$: the result for the energy dependence of the $\alpha(W)$ parameter was very similar to the one for the $\beta(W)$ parameter but with a worse total reduced χ^2 (1.62 against 1.03 of the density fit).

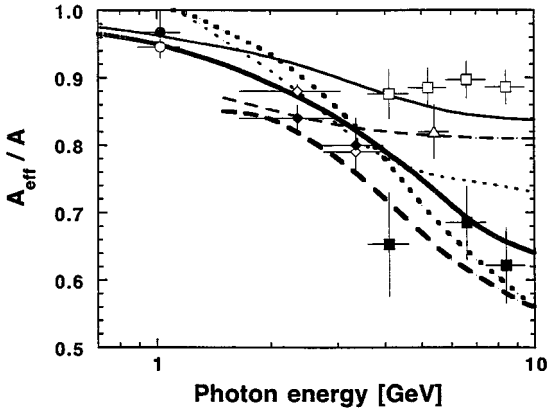

FIG. 11. Shadowing effect measured for C (open symbols) and Pb (solid symbols). Our data (circles) are shown together with some data available from literature: rhombs [37], triangles [40] and squares [39]. Lines are VMD different predictions: solid lines [38], dashed lines [20], and dotted lines [19]; thin and thick lines are the predictions for C and Pb, respectively.

For a more quantitative evaluation, the same procedure used to fit the average-nucleus cross-section data was employed to fit the data for the different nuclei, in order to extract δM_Δ, $\delta\Gamma_\Delta$, and $\delta\Gamma_{N*}$ for each nucleus. The results obtained are plotted in Figs. 13(a) and 13(b) versus the nuclear density: as it is seen a nice linear behavior is found in agreement with the prediction of the model [see Eqs. (11) and (12)].

Therefore it is reasonable to conclude that, due to the resonance propagation and interaction, in the photoabsorption on nuclei the Δ-resonance mass increases with the nuclear density up to few tenths of MeV, the Δ-resonance width up to several tenths of MeV, while the averaged N^*-resonance width up to few hundreds of MeV.

VI. CONCLUSION

We have measured the total photoabsorption cross section for several nuclei in the energy range 300–1200 MeV, using the photohadronic technique with a 4π NaI detector to detect hadronic events and a lead-glass counter to tag the electromagnetic ones. From the comparison between the new re-

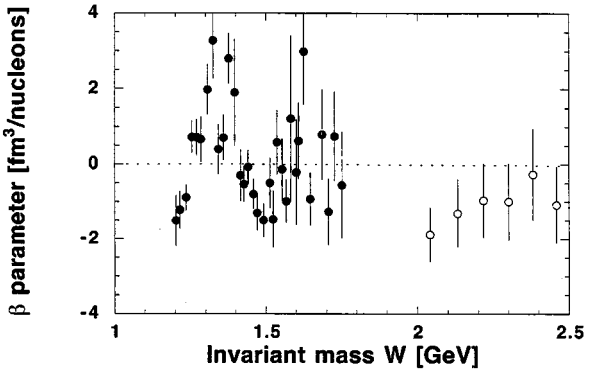

FIG. 12. Linear coefficient β derived for each invariant mass W from our data on Li, C, Al, Cu, Sn, and Pb (solid circles) and from Daresbury data on C, Al, Cu, Sn, and Pb (open circles).

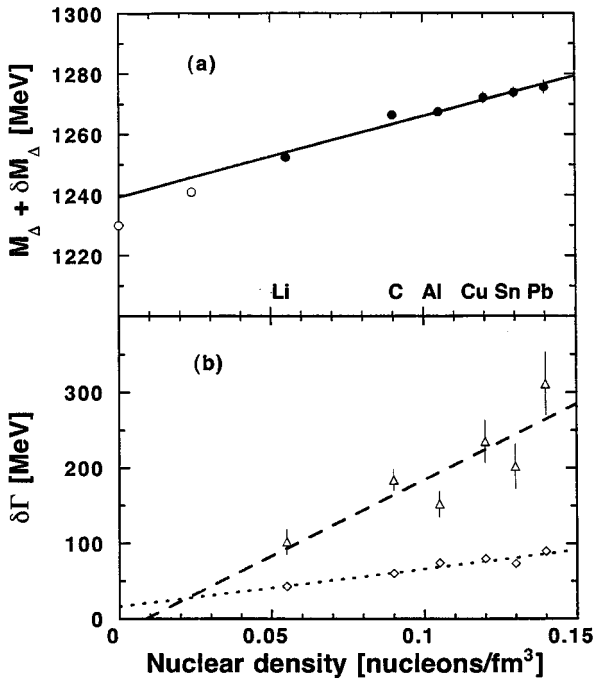

FIG. 13. (a) Mass of the Δ-resonance extracted from our data on nuclei (solid circles) and from hydrogen and deuterium data (open circles). The hydrogen density is arbitrarily assumed equal to 0. (b) Broadening due to interaction of the Δ-resonance (diamonds) and the average value for N^* resonances (triangles) extracted from our data. Lines are linear fits in the nuclear density.

sults for nuclei and previous data for the free nucleon, we deduced several effects due to the nuclear medium.

(a) The Δ-resonance mass and width increase almost linearly with the nuclear density. This means that Δ-resonance photoexcitation, like Δ-resonance hadron-excitation, has not an ''universal'' nuclear behavior.

(b) Nuclear medium effects produce a larger broadening of the peak for higher nucleon resonances. This broadening increases linearly with the nuclear density and can be explained in terms of a strong hadronic interaction in the propagation of the photoproduced resonances.

(c) At present, no realistic information can be extracted for the mass shifts of the higher resonances in nuclei. Being the nuclear medium effect large for the resonance widths, it would be interesting to look at the possible mass variations for different resonances.

(d) The systematic reduction of the cross section in nuclei above 600 MeV seems to require a reduction of the elementary coupling and this might be considered in terms of a partial depletion of higher nucleon resonance excitation strength and of the onset of the shadowing effect due to the low-mass component in the hadronic spectrum of the photon.

Clearly, detailed microscopic theoretical treatments of higher nucleon resonances, like those developed for the Δ resonance are urgently needed in order to describe the data in a less phenomenological framework. Also new experimental data are welcome to fill the existing gap between 1.2 and 1.8 GeV and give a more definitive answer on the threshold and the rising of the shadowing effect.

ACKNOWLEDGMENTS

We are pleased to thank our technicians M. Albicocco, A. Orlandi, W. Pesci, A. Rottura, and A. Viticchie for their continuous technical assistance and the ADONE staff for the efficiency in running the machine. We are grateful to L. A. Kondratyuk for many useful discussions and to G. Piller, W. Ratzka, and W. Weise for providing us with the result of their calculation prior to publication. Finally we thank P. Pedroni for providing us with the data collected at Mainz.

[1] J. Ahrens, Nucl. Phys. **A446**, 229c (1985), and reference therein.
[2] J. H. Koch, E. J. Moniz, and N. Ohtsuka, Ann. Phys. (NY) **154**, 99 (1984).
[3] A. S. Carrol *et al.*, Phys. Rev. C **14**, 635 (1976).
[4] E. A. Arakelyan *et al.*, Sov. J. Nucl. Phys. **38**, 589 (1983).
[5] A. K. Ananikyan *et al.*, Sov. J. Nucl. Phys. **46**, 208 (1987).
[6] N. Bianchi *et al.*, Phys. Lett. B **299**, 219 (1993).
[7] M. Anghinolfi *et al.*, Phys. Rev. C **47**, R922 (1993).
[8] N. Bianchi *et al.*, Phys. Lett. B **309**, 5 (1993).
[9] T. A. Armstrong *et al.*, Phys. Rev. D **5**, 1640 (1972).
[10] T. A. Armstrong *et al.*, Nucl. Phys. **B41**, 445 (1972).
[11] Th. Frommhold, F. Steiper, W. Henkel, U. Kneissl, J. Ahrens, R. Beck, J. Peise, and M. Schmitz, Phys. Lett. B **295**, 28 (1992).
[12] Th. Frommhold *et al.*, Z. Phys. A **350**, 249 (1994).
[13] N. Bianchi *et al.*, Phys. Lett. B **325**, 333 (1994).
[14] R. C. Carrasco and E. Oset, Nucl. Phys. **A536**, 445 (1992).
[15] L. Kondratyuk, M. I. Krivoruchenko, N. Bianchi, E. De Sanctis, and V. Muccifora, Nucl. Phys. **A579**, 453 (1994).
[16] W. M. Alberico, G. Gervino, and A. Lavagno, Phys. Lett. B **321**, 177 (1994).
[17] M. M. Giannini and E. Santopinto, Phys. Rev. C **49**, 1258 (1994).
[18] S. V. Akulinichev and A. I. L'vov, Mainz Internal Report MKPH-T-93-1.
[19] S. J. Brodsky and J. Pumplin, Phys. Rev. **182**, 1794 (1969).
[20] K. Gottfried and D. R. Yennie, Phys. Rev. **182**, 1595 (1969).
[21] P. Distas and G. Shaw, Nucl. Phys. **113**, 246 (1976).
[22] G. Shaw, Phys. Rev. D **47**, R3676 (1993).
[23] G. Piller and W. Weise, Phys. Rev. C **42**, 1834 (1990).
[24] W. Weise, Phys. Rev. Lett. **31**, 773 (1973); Phys. Rep. **13**, 53 (1974).
[25] N. Bianchi *et al.*, Nucl. Instrum. Methods Phys. Res. A **311**, 173 (1992).
[26] N. Bianchi *et al.*, Frascati Internal Report LNF 95/093.
[27] V. S. Barashenkov *et al.*, Nucl. Phys. **A231**, 462 (1974).
[28] V. Muccifora *et al.*, Nucl. Instrum. Methods Phys. Res. A **332**, 288 (1993).

[29] M. Mac Cormick *et al.*, Phys. Rev. C **53**, 41 (1996).
[30] R. L. Walker *et al.*, Phys. Rev. **182**, 1729 (1969).
[31] H. Arenhövel *et al.*, Nucl. Phys. **A374**, 521c (1982).
[32] Particle Data Group, K. Hikasa *et al.*, Phys. Rev. D **45**, S1 (1992), pp. 11.25–11.27.
[33] A. Leprètre *et al.*, Nucl. Phys. **A367**, 23 (1981).
[34] J. Ahrens *et al.*, in *Proceedings of the International Conference on High Energy Physics and Nuclear Structure* Vancouver, 1979, edited by D. F. Measday and A. W. Thomas (North-Holland, Amsterdam, 1980), p. 67.
[35] J. Arends, J. Eyink, A. Hegerath, K. G. Hilger, B. Mecking, G. Noldeke, and H. Rost, Phys. Lett. **98B**, 423 (1981).
[36] P. Carlos, in *Proceedings of the International School of Intermediate Energy Nuclear Physics*, Verona, 1985, edited by R. Bergère, S. Costa, and C. Schaerf (World Scientific, Singapore, 1985), p. 1.
[37] G. R. Brookes *et al.*, Phys. Rev. D **8**, 2826 (1973).
[38] G. Piller, W. Ratzka, and W. Weise, private communication.
[39] D. O. Caldwell, V. B. Elings, W. P. Hesse, R. J. Morrison, F. V. Murphy, and D. E. Yount, Phys. Rev. D **7**, 1362 (1973).
[40] V. Heynen, H. Meyer, B. Naroska, and D. Notz, Phys. Lett. **34B**, 651 (1971).
[41] C. W. De Jager, H. De Vries, and C. De Vries, At. Data Nucl. Data Tables **14**, 479 (1974).